



**HAL**  
open science

## Study of hot tearing and macrosegregation through ingot bending test and its numerical simulation

Takao Koshikawa, Michel Bellet, Charles-André Gandin, Hideaki Yamamura,  
Manuel Bobadilla

► **To cite this version:**

Takao Koshikawa, Michel Bellet, Charles-André Gandin, Hideaki Yamamura, Manuel Bobadilla. Study of hot tearing and macrosegregation through ingot bending test and its numerical simulation. MCWASP XIV: International Conference on Modelling of Casting, Welding and Advanced Solidification Processes, Jun 2015, Awaji island, Hyogo, Japan. pp.012096, 10.1088/1757-899X/84/1/012096 . hal-01254355

**HAL Id: hal-01254355**

**<https://minesparis-psl.hal.science/hal-01254355>**

Submitted on 12 Jan 2016

**HAL** is a multi-disciplinary open access archive for the deposit and dissemination of scientific research documents, whether they are published or not. The documents may come from teaching and research institutions in France or abroad, or from public or private research centers.

L'archive ouverte pluridisciplinaire **HAL**, est destinée au dépôt et à la diffusion de documents scientifiques de niveau recherche, publiés ou non, émanant des établissements d'enseignement et de recherche français ou étrangers, des laboratoires publics ou privés.

# Study of hot tearing and macrosegregation through ingot bending test and its numerical simulation

T Koshikawa<sup>1,2</sup>, M Bellet<sup>1</sup>, C A Gandin<sup>1</sup>, H Yamamura<sup>3</sup> and M Bobadilla<sup>4</sup>

<sup>1</sup> MINES ParisTech & CNRS, CEMEF UMR 7635, 06904 Sophia Antipolis, France

<sup>2</sup> Nippon Steel & Sumitomo Metal Corporation, Oita Works Equipment Division, 1 Oaza-Nishinosu, Oita City 870-0992, Japan

<sup>3</sup> The Japan Institute of Metals and Materials, 1-14-32, Ichibancho, Aoba-ku, Sendai 980-8544, Japan

<sup>4</sup> ArcelorMittal Maizières, Research and Development, BP 30320, 57283 Maizières-lès-Metz, France

E-mail: koshikawa.4eb.takao@jp.nssmc.com

**Abstract.** Ingot bending tests are performed on the already formed solid shell of a 450 kg solidifying ingot. It is designed in order to be representative of two defects occurring during secondary cooling in steel continuous casting: hot tearing and macrosegregation. Ingots show the defects which result from the application of bending. In order to understand the different physical phenomena, finite element numerical modelling of the test has been developed, using two different approaches. A first approach consists of a 3D finite element thermomechanical simulation. Hot tearing criteria, based on strain, strain rate and two values for solid fraction are then evaluated. It is demonstrated that such a strain based criterion has an excellent capability to predict the formation of hot tears. A second approach consists of a 2D planar finite element simulation in the median section of the ingot. A two-phase formulation is used, in which the velocity of the liquid and solid phases are distinguished. The simulation shows how solutes are redistributed through the ingot under the effect of bending. Solute-depleted and enriched regions are well reproduced, but peak values of macrosegregation are underestimated.

## 1. Introduction

The paper focuses on two major defects encountered during secondary cooling in steel Continuous Casting (CC): hot tearing and macrosegregation.

Hot tearing or hot cracking takes place deep in the mushy zone, close to the end of solidification, typically for solid fractions over 0.9 when the material is subject to tensile strains and stresses. In CC this happens during the bending or unbending of the strand, or as a consequence of bulging of the shell between support rolls under the effect of metallostatic pressure. In this study, the macroscopic hot tearing criterion proposed by Won et al. [1] is evaluated. Being interpreted like in [2], this criterion is based on cumulated strain perpendicular to dendrite growth direction. The corresponding strain rate is denoted  $\hat{\varepsilon}$ . The strain based criterion,  $HCC_{WYSO}$ , is then expressed as follows:

$$HCC_{WYSO} = \left( \int_{BTR} \hat{\varepsilon} dt - \hat{\varepsilon}_C \right) \text{ with } \hat{\varepsilon}_C = \frac{\varphi}{(\hat{\varepsilon})^{m^*} BTR^{n^*}} \quad (1)$$



where  $\hat{\epsilon}_c$  is the strain limit which depends itself on the perpendicular strain rate and on the Brittle Temperature Range (BTR). As this BTR is defined by two characteristic solid fractions (typically 0.9 and 1.0), it depends on the solidification path and thus both micro and macrosegregation are expected to affect hot tearing sensitivity. The three other parameters deduced in [1] from non-linear data fitting with several hot tearing experiments are:  $\phi = 0.02821$ ,  $m^* = 0.3131$ ,  $n^* = 0.8638$ .

Another critical defect in CC products is macrosegregation. It is observed at the centre of the slab. The principal cause is the relative movement of the liquid phase with respect to the solid phase. In CC, as mentioned above, bulging of the solid shell between support rolls and bending and unbending of the strand have an impact on the generation of such relative movement and hence on macrosegregation.

In order to identify those defects, an experiment, so-called ingot bending test, has been developed by several researchers [3-8]. The present tests have been designed and operated by Nippon Steel and Sumitomo Metal Corporation [9, 10]. For analyzing the tests, finite element numerical simulation of the tests has been developed using the commercial package THERCAST<sup>®</sup>. The location and occurrence of hot tears and macrosegregation are explained and discussed based on the simulations.

## 2. Ingot bending test

The schematic of the ingot bending test is shown in Figure 1. It has been designed to mimic the thermomechanical solicitations taking place during CC process; for instance, with respect to the evolution of the cooling rate and deformation. The procedure of the experiment is as follows: the molten metal is prepared in a ladle and the temperature is maintained at 1640 °C before pouring. The molten metal is filled into the mold from the top through a tundish. The filling duration is about 70 s. After filling, powder is added at the top of the ingot to limit heat exchanges with the air. The mass of metal is approximately 450 kg. The size of the ingot is 0.16 m thick, 0.5 m width and 0.75 m height. At a precise time after filling, the upper part of one of the two large faces of the mold is removed. The ingot is then deformed during solidification by pushing a horizontal cylindrical tool on the surface of the ingot, its longitudinal axis being located 0.45 m from the bottom of the ingot. The tool velocity and displacement are controlled by means of a hydraulic system and measured during the test. The reaction force is also measured using the time evolution of the hydraulic system pressure. The test conditions referred to as N-1 to N-6 are summarized in Table 1, together with measured nominal compositions in the ladle before filling. Note that a unique alloy composition was targeted for the experimental results reported hereafter. To know temperature evolution during the test, thermocouples are positioned in the ingot and the fixed large face of the mold. Furthermore, the ingot surface temperature has been measured with a pyrometer in test N-4 before and after deformation after partial mold removal. After the experiment, the ingot was cut and micrographs were investigated after appropriate etching to investigate hot tearing occurrence, intensity and location.

## 3. Thermomechanical modeling

### 3.1. Standard thermo-mechanical modeling

In the standard thermomechanical modelling approach [11, 12], the mushy zone (composed of liquid and solid phases) is considered as a homogenized continuum so that a unique velocity field is solved for. The numerical simulation is based on thermomechanical stress/strain analysis. It is conducted using the 3D finite element code THERCAST<sup>®</sup>. The thermal problem and the mechanical problem are solved sequentially at each time increment. The solidification path is defined a priori [13]. The alloy is modeled with a hybrid constitutive equation: over the solidus temperature, the alloy is seen as a non-Newtonian fluid obeying a temperature-dependent viscoplastic law. Below solidus, an elastic-viscoplastic behavior is used with strain hardening considered through a multiplicative law [11, 12].

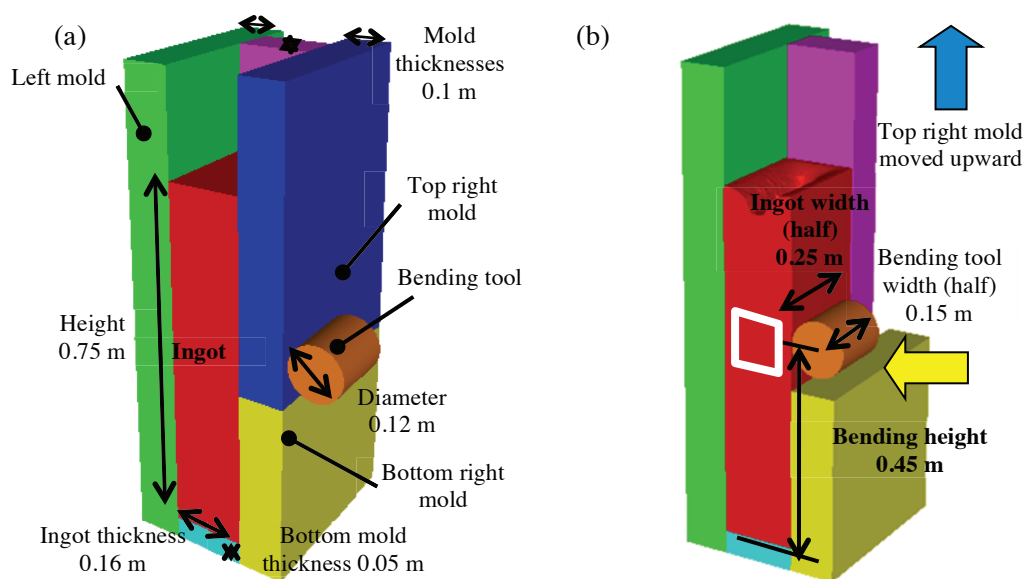


**Figure 1.** Schematic of the hot tearing experiment developed at Nippon Steel & Sumitomo Metal Corporation showing (a) initial state and (b) bending stage after partial mold removal. The configuration shown is half of the setup, considering symmetry with respect to the central transverse cut through the ingot, mold and bending tool domains.

**Table 1.** Measured nominal compositions and experimental conditions.

	Nominal composition (mass%)						Mold removal (s)	Bending start (s)	Displace- ment (mm)	Velocity (mm s <sup>-1</sup> )
	C	Si	Mn	P	S	Al				
N-1	0.20	0.22	1.50	0.021	0.007	0.039	590	792	13	2.0
N-2	0.20	0.20	1.47	0.020	0.010	0.038	450	574	6	2.0
N-3	0.19	0.24	1.50	0.022	0.010	0.064	457	517	6	1.0
N-4	0.19	0.21	1.49	0.021	0.010	0.064	300	499	6	0.5
N-5	0.19	0.21	1.50	0.020	0.010	0.041	321	510	6	0.25
N-6	0.20	0.21	1.48	0.021	0.010	0.055	340	510	3	0.25

Concerning solidification, three microsegregation paths are used. The first one is based on the lever rule (LR) approximation, meaning that full thermodynamic equilibrium is assumed in all existing phases at any temperature. The second one is a combination of the partial-equilibrium approximation together with the para-equilibrium approximation (PE+PA) in which an interstitial element (e.g., carbon) has infinite diffusivity in all phases whereas substitutional elements are frozen in solid phases. In addition, the PE+PA approximation accounts for the peritectic reaction taking place in the steel grade investigated in this study. The last solidification path (EX) is extracted from measurements conducted on a simple unidirectional solidification experiment. The details of these approximations and the solidification for alloy similar alloy compositions are given in reference [13, 14].

As illustrated in Figure 1, the 3D numerical domains are described considering the symmetry of the setup. Filling stage is not taken into account so that the thermo mechanical simulation starts 70 s after filling. The initial temperature of the ingot, 1550 °C, is estimated using measurements. It is set to 20 °C for all other domains. The thermal boundary condition in between ingot and mold is defined as an air gap dependent heat resistance. When the ingot is into contact with the mold, the heat transfer

coefficient is calibrated with measurement and set to  $850 \text{ W m}^{-2} \text{ K}^{-1}$ . When air gap generates, its width is considered and a heat exchange coefficient is computed between the ingot and the mold surfaces. It takes into account radiation and heat conduction in the air. Regarding the ingot top, adiabatic condition is used. After mold removal, the free surface heat exchange as accounts for radiation and convection, with the values for emissivity and convective heat transfer coefficient taken as 0.8 and as  $15 \text{ W m}^{-2} \text{ K}^{-1}$ , respectively. This standard thermo-mechanical simulation is carried out for test N-2 to N-6, which is focused on hot tearing study.

### 3.2. “Two-phase” modeling and macrosegregation analysis

The second approach is an effective “two-phase” modeling in which liquid and solid velocity fields are considered separately and solved concurrently in the mushy zone. It allows simulating solute transport phenomena leading to macrosegregation induced by deformation, shrinkage and advection. It is performed with the 2D finite element code R2SOL. Details of the formulation can be found in references [14, 15].

Concerning solidification path, it is not defined a priori since solute composition varies due to solute transport. To model the microsegregation phenomena, the lever rule approximation is considered for a multi component system assuming constant partition coefficients and liquidus slopes for each solute element. Those physical properties are obtained using Thermocalc with TCFE6 database, shown in Table 2. Fusion temperature is defined as  $1538 \text{ }^\circ\text{C}$ . Regarding with permeability, Carman-Kozeny model is employed. The secondary dendrite arm spacing is predefined as  $300 \text{ }\mu\text{m}$  measured in the micrograph in case of N-1.

This effective two-phase modeling is applied to test N-1, in which the ingot centre is fully mushy when bending starts (Table 1). The calculation is carried out in two steps. At first, a standard thermomechanical calculation is conducted up to the bending stage. The simulation is then started again using the “two-phase” model. As a consequence, it is assumed that there is no macrosegregation at the beginning of this second two-phase simulation.

**Table 2.** Partition coefficient and liquidus slope for each solutes.

	C	Si	Mn	P	S
Partition coefficient	0.162	0.639	0.703	0.282	0.027
Liquidus slope (K/wt%)	-81	-12	-5	-29	-34

## 4. Results and discussion

### 4.1. Standard thermo-mechanical simulation result

#### 4.1.1. Temperature evolution for test N-4

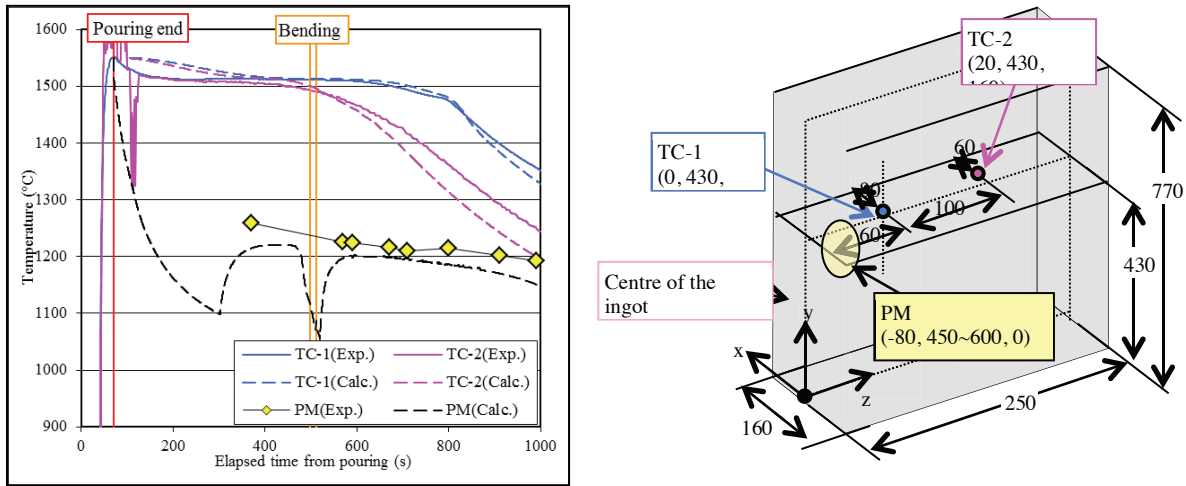
Figure 2 shows the comparison of temperature evolution in the ingot. There are two thermocouples in the ingot. TC-1 is close to the ingot center (blue line in Figure 2) while TC-2 is located close to the narrow face of the ingot (pink line in Figure 2). In addition, measured surface temperature evolution at the height of the bending tool is plotted (yellow diamond-shape in Figure 2). At 300 s, the mold located in front of the bending tool is removed prior to bending (Table 1). Consequently, the surface temperature increases. The calculated temperature evolution is in good agreement with measured data. Thermal modeling regarding the boundary condition and thermo physical parameters are thus well calibrated from about 300 s. Before this time, cooling curves in Figure 2 reveal overestimation of the predicted temperatures. This is due to the choice not to model the filling stage.

#### 4.1.2. Reaction force comparison for test N-4

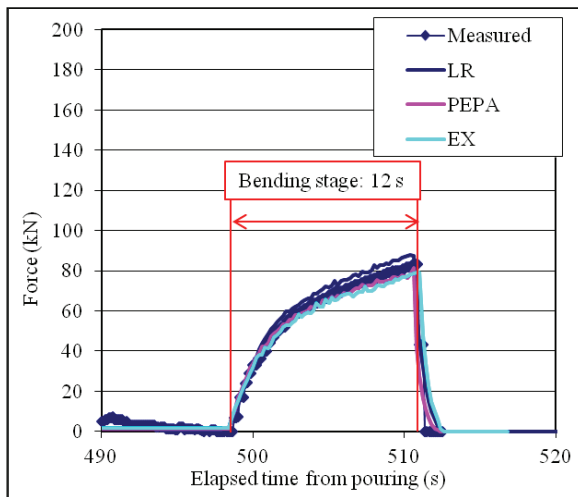
Figure 3 shows the comparison of the reaction force evolution during the bending stage for N-4. Good agreement is found between measurements and simulations. This indicates that the thermomechanical modeling works well, leading to good stress and strain field predictions. The microsegregation effect does not clearly appear although the LR approximation shows greater force than the two others. This is linked to the difference of the solid shell thickness at the time when bending is applied.

4.1.3. Hot tearing prediction using strain based criterion

Figure 4a shows a typical micrograph for experiment N-6 close to the bending region identified with a white rectangle in Figure 1b. In case of N-6, the surface deformation due to bending is not so clear. One can see a dendritic microstructure which grew from the ingot surface (right hand side) toward the centre of the ingot (left hand side). Around the center of the ingot, the morphology is changed to equiaxed, which is due to the decrease of the temperature gradient close to the center of the ingot. In the micrograph, hot tears are found in interdendritic regions.

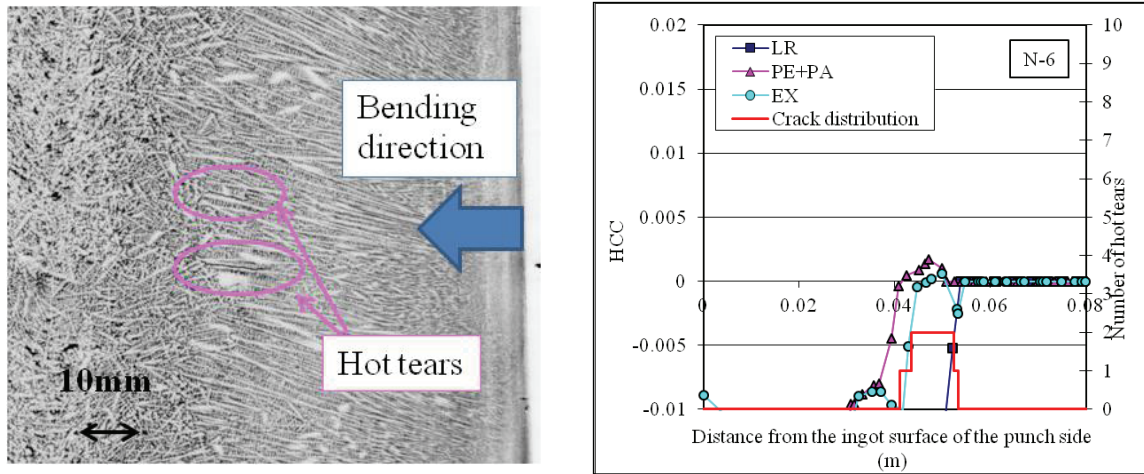


**Figure 2.** Comparison of temperature evolution in the ingot and schematic showing position of thermocouple TC-1 and TC-2 in the ingot, as well as the position at the ingot surface where pyrometer PM records the temperature after partial mold removal.

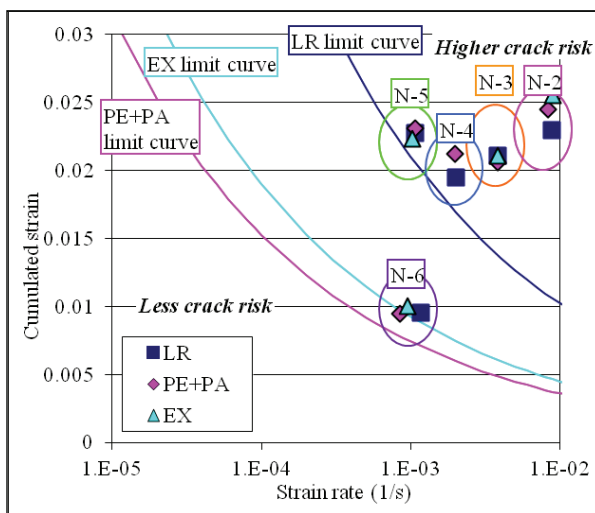


**Figure 3.** Force evolution during bending stage for trial N-4 deduced from measurements and from simulations using the three microsegregation models.

Figure 4b shows a comparison of the hot tearing sensitivity profile defined with Eq. (1) at the bending tool height for the three microsegregation models. In addition, the crack location is superimposed on the profile. The position of the crack location is in good agreement with two microsegregation cases; PE+PA and EX, with HCC reaching positive values between 0.04 m and 0.05 m from the ingot surface of the punched side. In contrast, the profile using LR shows negative values at the crack position. These results clearly reveal the critical role played by the microsegregation model on hot tearing prediction.



**Figure 4.** A micrograph of test N-6 and the comparison of the hot tearing sensitivity profile with the location of the hot tears in the bending region. Hot tearing sensitivity is calculated with the three microsegregation models.



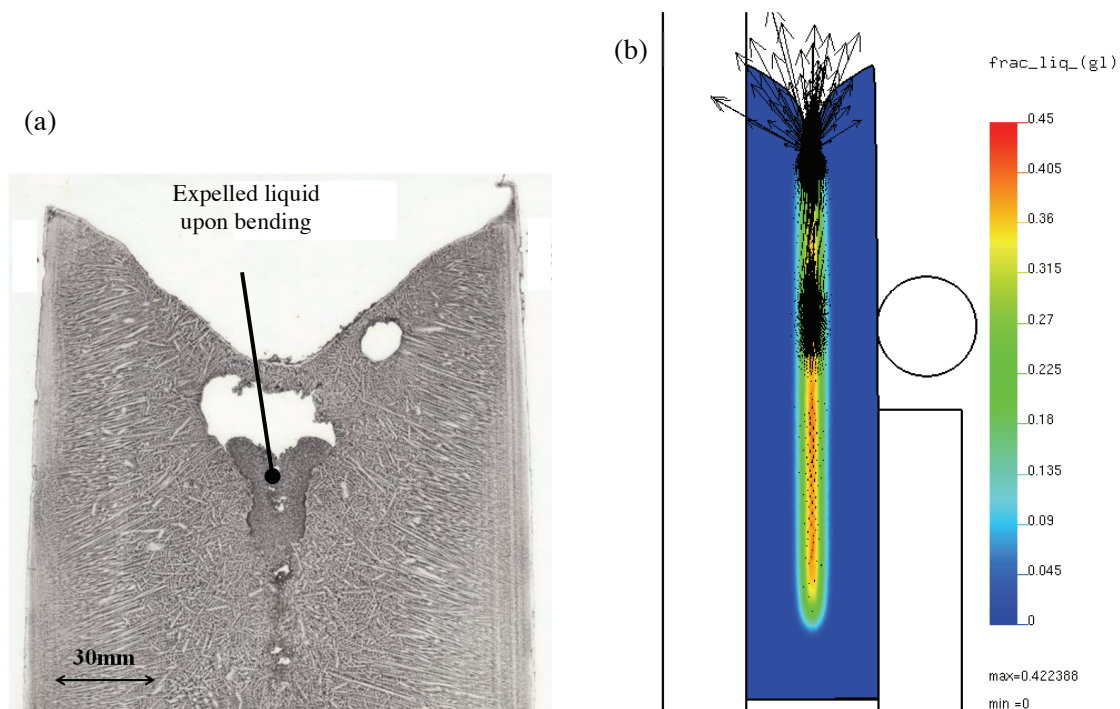
**Figure 5.** Computed cumulated strain,  $\int_{BTR} \hat{\epsilon} dt$ , as a function of the maximum perpendicular strain rate calculated when passing through the BTR. Values taken from the  $HCC_{WYSO}$  profile at the bending height, an example being shown in Figure 4b. The three continuous curves indicate the strain limit  $\hat{\epsilon}_C$  (Eq. 1).

Figure 5 presents limit curves based on the three microsegregation models. The continuous curves correspond to the strain limit that constitutes the second term of the WYSO criterion in Eq. (1):  $\hat{\epsilon}_C = \varphi \hat{\epsilon}^{-m^*} BTR^{-n^*}$ . The different values of the BTR for LR, EX and PE+PA explain the 3 limits. For each curve, the top right domain corresponds to  $HCC_{WYSO} > 0$ , thus presenting a higher crack risk. According to its smaller BTR, the LR limit curve is placed on the top right region of the graph. Calculated values are superimposed on the figure for trials N-2 to N-6. To this end, the profile of the cumulated perpendicular strain and strain rate are drawn along the thickness of the ingot at the bending tool height. The maximum cumulated strain is taken from the profile as well as the corresponding value for the perpendicular strain rate. These are the two variables used to express local values of  $HCC_{WYSO}$  from Eq. (1) and then plot the simulation results in Figure 5. The distribution of the results in the graph is linked to the applied displacement and velocity of the bending tool shown in Table 1. It is found that the microsegregation model does not have a major impact on the cumulated strain and maximum strain rate in the BTR since the three points for each trial are very close. Note that, while metallographic investigations of all these trials have revealed the presence of hot tears, only the PE+PA and EX curves give a good response. The simulation using LR does not work as N-6 is not located in the high crack risk region.

## 4.2. “Two-phase” simulation result

### 4.2.1. Liquid phase velocity field during bending

Figure 6a shows a micrograph of trial N-1 at the ingot top. It is seen that the different microstructure coming from different cooling effect is observed at the top center. Interpretation is that, due to bending, remaining melt is expelled from the mushy core in the bending region towards the top of the ingot. This is explained in the simulation result presented in Figure 6b. It is found that bending generates an upward flow toward the ingot top region. The boundary of the top is not fully solidified so that the melt goes out and covers the already formed solid shell. Figure 6a clearly shows this effect. It can be seen that the two-phase numerical modeling is able to retrieve this phenomenon.



**Figure 6.** On the left, a micrograph of the ingot top for test N-1 shows the structure of the top ingot resulting from an expulsion of liquid upon bending: some liquid entered the primary shrinkage macrocavity. On the right, simulated relative velocity vectors in the liquid phase are superimposed on the liquid fraction field for trial N-1, showing the same phenomenon during bending.

### 4.2.2. Comparison for macrosegregation

Figure 7 shows a micrograph of trial N-1 close to the bending region, the print of the bending tool being visible on the right-hand-side of the ingot surface. A white vertical band is seen at the center of the ingot. It reveals clear negative segregation of Mn, which would result from the deformation of the mushy region. A similar profile was obtained for P. Figure 7 also shows the comparison of the relative concentration profile of Mn along the dashed line superimposed to the micrograph at the bending height. The calculated negative segregation is not enough marked compared to the measurement result. There are several possible causes for this difference, among which approximate microsegregation modeling, inaccurate knowledge of rheological parameters, mush permeability, thermodynamic and thermophysical data.

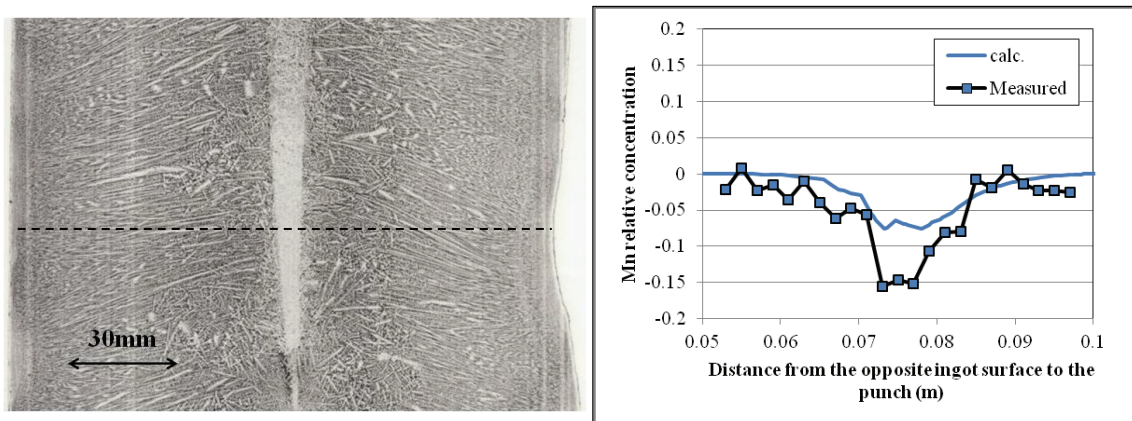


**Figure 7.** A micrograph of the ingot bending region for the test N-1 and comparison of Mn relative concentration profile at bending height with measurement result by means of EPMA. Simulation results show qualitative agreement with measurements.

## 5. Conclusion

An ingot bending test has been developed and modeled using two numerical codes. Using a standard thermomechanical model, it is found that strain based criteria have capability to predict crack occurrence and location. In addition, the microsegregation model or solidification path has an impact on the predicted hot tearing sensitivity. Through effective “two-phase” simulation, qualitative agreement with respect to liquid flow and its consequent negative segregation at ingot centre is demonstrated. However, the amplitude of negative segregation is found smaller than the measurement result. Further sensitivity analyses would be useful to understand this discrepancy and reach a better quantitative agreement.

## Acknowledgments

This work is supported by Nippon Steel & Sumitomo Metal Corporation in a collaborative project with ArcelorMittal. The authors are deeply grateful to Drs Olivier Jaouen and Frederic Costes from Transvalor SA (Mougins, France), for their kind help and discussion about thermomechanical modeling using THERCAST<sup>®</sup> software.

## References

- [1] Won Y M, Yeo T -J, Seol D J and Oh K H 2000 *Mater. Trans. B* **31** 779
- [2] Bellet M, Cerri O, Bobadilla M and Chastel Y 2009 *Mater. Trans. A* **40** 2705
- [3] Sato H, Kitagawa T, Murakami K and Kawawa T 1975 *Tetsu to Hagane* **61** S471
- [4] Miyamura K, Ochi A, Kanamaru K and Kaneko N 1976 *Tetsu to Hagane* **62** S482
- [5] Marukawa K, Kawasaki M, Kimura T and Ishimura S 1978 *Tetsu to Hagane* **64** S661
- [6] Narita K, Mori T, Ayata K, Miyazaki J and Fujimaki M 1978 *Tetsu to Hagane* **64** S152
- [7] Sugitani Y, Nakamura M, Kawashima H and Kawasaki M 1980 *Tetsu to Hagane* **66** S193
- [8] Wintz M, Bobadilla M and Jolivet J M 1994 *La Rev. Métall.* **4** 105
- [9] Murao T, Kajitani T, Yamamura H, Anzai K, Oikawa K and Sawada T 2013 *Tetsu to Hagane* **99** 94
- [10] Murao T, Kajitani T, Yamamura H, Anzai K, Oikawa K and Sawada T 2014 *ISIJ* **54** 359
- [11] Bellet M, Jaouen O and Poittraut I 2005 *Int. J. Num. Meth. Heat Fluid Flow* **15** 120
- [12] Bellet M and Fachinotti V D 2004 *Comput. Meth. Appl. Mech. Eng.* **193** 4
- [13] Koshikawa T, Gandin Ch- A, Bellet M, Yamamura H and Bobadilla M 2014 *ISIJ* **54** 1274
- [14] Koshikawa T, Bellet M, Yamamura H and Bobadilla M 2013 *STEELSIM2013 (Ostrava, Czech Republic, 10-12 September 2013)* topic 5
- [15] Fachinotti V D, Le Corre S, Triolet N, Bobadilla M and Bellet M 2006 *Int. J. Num. Meth. Eng.* **67** 1341